PNAS RESEARCH ARTICLE | IMMUNOLOGY AND INFLAMMATION

Palmitoylation at a conserved cysteine residue facilitates gasdermin D-mediated pyroptosis and cytokine release

Zhonghua Liu[a,b,1,2], Sai Li[a,b,1], Chuanping Wang[a], Kaylynn J. Vidmar[a], Syrena Bracey[a], Ling Li[c], Belinda Willard[c], Masaru Miyagi[d], Tong Lan[e], Bryan C. Dickinson[e], Abdullah Osme[a,3], Theresa T. Pizarro[a], and Tsan Sam Xiao[a,2]

Affiliations are included on p. 10.

Edited by Katherine Fitzgerald, University of Massachusetts Medical School, Worcester, MA; received January 15, 2024; accepted June 6, 2024

Gasdermin D (GSDMD)-mediated pyroptotic cell death drives inflammatory cytokine release and downstream immune responses upon inflammasome activation, which play important roles in host defense and inflammatory disorders. Upon activation by proteases, the GSDMD N-terminal domain (NTD) undergoes oligomerization and membrane translocation in the presence of lipids to assemble pores. Despite intensive studies, the molecular events underlying the transition of GSDMD from an autoinhibited soluble form to an oligomeric pore form inserted into the membrane remain incompletely understood. Previous work characterized *S*-palmitoylation for gasdermins from bacteria, fungi, invertebrates, as well as mammalian gasdermin E (GSDME). Here, we report that a conserved residue Cys191 in human GSDMD was *S*-palmitoylated, which promoted GSDMD-mediated pyroptosis and cytokine release. Mutation of Cys191 or treatment with palmitoyltransferase inhibitors cyano-myracrylamide (CMA) or 2-bromopalmitate (2BP) suppressed GSDMD palmitoylation, its localization to the membrane and dampened pyroptosis or IL-1β secretion. Furthermore, *Gsdmd*-dependent inflammatory responses were alleviated by inhibition of palmitoylation in vivo. By contrast, coexpression of GSDMD with palmitoyltransferases enhanced pyroptotic cell death, while introduction of exogenous palmitoylation sequences fully restored pyroptotic activities to the C191A mutant, suggesting that palmitoylation-mediated membrane localization may be distinct from other molecular events such as GSDMD conformational change during pore assembly. Collectively, our study suggests that *S*-palmitoylation may be a shared regulatory mechanism for GSDMD and other gasdermins, which points to potential avenues for therapeutically targeting *S*-palmitoylation of gasdermins in inflammatory disorders.

gasdermin D | pyroptosis | *S*-palmitoylation | ZDHHC palmitoyltransferase | inflammasome

Significance

Pyroptosis is an inflammatory form of cell death that plays important roles in host defense and inflammatory disorders. Despite intensive studies, the molecular events underlying the gasdermin D (GSDMD)-mediated pyroptosis remain poorly understood. Previous work characterized *S*-palmitoylation for gasdermins from bacteria, fungi, invertebrates, as well as mammalian GSDME. Here, we report that a conserved residue Cys191 in human GSDMD was *S*-palmitoylated, which promoted GSDMD-mediated pyroptosis and cytokine release through membrane localization. Our work suggests that palmitoylation may be a shared regulatory mechanism for this family of pore-forming proteins that transition from autoinhibited soluble forms to oligomeric pore forms inserted into the membrane and points to avenues for therapeutically targeting *S*-palmitoylation of gasdermins in inflammatory disorders.

The inflammasomes are crucial innate immune signaling platforms implicated in immune defense against infections and autoimmune/autoinflammatory disorders such as multiple sclerosis and Alzheimer's disease (1–3). Activation of the inflammasomes may lead to the maturation and secretion of proinflammatory cytokines IL-1β and IL-18, as well as pyroptosis, a highly inflammatory form of lytic cell death mediated by gasdermin D (GSDMD) (4–6). GSDMD belongs to a family of six paralogs GSDMA-GSDME and DFNB59 (Pejvakin) (7, 8). Most of these proteins reside in autoinhibited conformations through intramolecular association of their N- and C-terminal domains (NTDs and CTDs). Upon activation of the inflammasome pathways, GSDMD is cleaved by inflammatory caspases-1, 4, 5, and 11 at its linker between NTD and CTD. This facilitates the release of the NTD–CTD autoinhibition in the presence of phospholipids, which in turn catalyzes drastic conformational changes in the NTDs. Perhaps concurrently, the NTDs translocate to the membrane, oligomerize, and assemble membrane pores to induce lytic cell death (9–15). In addition to cleavage by inflammatory caspases, GSDMD can be processed by caspase-8, neutrophil elastase (ELANE), and cathepsin G to induce pyroptosis (16–20). Such lytic cell death facilitates the release of intracellular contents such as cytokines and other danger signals, which in turn recruit other immune cells to amplify and perpetuate inflammation. As such, pyroptosis may function as an immune defense mechanism against infections through the exposure of intracellular pathogens to extracellular environment conducive to microbial killing (9, 10, 21–23); on the other hand, uncontrolled pyroptosis plays a major role in septic shock (24–28) and other inflammatory disorders (29, 30). Therefore, regulation of gasdermin-mediated pyroptosis has important implications in various pathological conditions.

Even though protease processing is the most intensively studied mechanisms of gasdermin regulation, emerging evidence suggests that gasdermins are modulated by other

The authors declare no competing interest.

This article is a PNAS Direct Submission.

[1]Z.L. and S.L. contributed equally to this work.

[2]To whom correspondence may be addressed. Email: xixiaolu@mail.ustc.edu.cn or tsx@case.edu.

[3]Present address: Department of Pathology, Heersink School of Medicine, University of Alabama at Birmingham, Birmingham, AL 35249.

This article contains supporting information online at https://www.pnas.org/lookup/suppl/doi:10.1073/pnas.2400883121/-/DCSupplemental.

Published July 9, 2024.

posttranslational modifications. For example, human GSDMB (hGSDMB, absent in rodents) and hGSDMD are ubiquitinated and marked for proteasome degradation by a bacterial E3 ligase invasion plasmid antigen H 7.8 (IpaH7.8) (31, 32). This serves as an immune evasion strategy for pathogens such as *Shigella flexneri*. Yet another mechanism of gasdermin regulation was suggested for GSDME and microbial gasdermin homologs. GSDME was reported to be *S*-palmitoylated at two Cys residues (33). Mutation of the palmitoylation sites or suppression of palmitoylation through 2BP treatment diminished pyroptosis induced by caspase-3 cleavage (33). In addition to cysteine *S*-palmitoylation in mammalian GSDME, a cysteine residue conserved in bacterial and fungal gasdermin homologs was shown to be *S*-palmitoylated and function in antiphage defense, as illustrated in a bacterial gasdermin structure (34). In the above cases, palmitoylation facilitates pore formation by gasdermins through either release of NTD–CTD autoinhibition or stabilization of the gasdermin structure. Whether palmitoylation plays other roles in gasdermin regulation remains to be elucidated.

Similar to GSDME and microbial gasdermins, Cys modifications in GSDMD have been suggested by several groups although the molecular mechanisms remain ill defined. Shortly after the discovery of GSDMD as a pyroptosis effector, a cysteine residue conserved among GSDMDs from different species (Cys191 in hGSDMD and Cys192 in mGSDMD) was reported to be important for pyroptotic activities (10). In agreement, we and others have shown that mutation of hGSDMD Cys191 or mGSDMD C192 led to impaired LDH release and/or PI uptake, suggesting that the process of pyroptosis was diminished in the absence of this conserved cysteine residue (35–37). On the other hand, structural studies have revealed that Cys191 is not in close proximity to other cysteines or each other in either the resting state or the oligomeric pore structure, thus unlikely to form disulfides (15, 38, 39). Small molecule compounds such as necrosulfonamide (35) or disulfiram (36) have been reported to covalently modify Cys191 to inhibit hGSDMD-mediated pyroptosis. Furthermore, Cys191 in hGSDMD and Cys192 in mGSDMD were shown to be covalently modified by fumarate (40), a tricarboxylic acid (TCA) cycle intermediate. This modification is referred to as succination, which suppresses GSDMD processing, oligomerization, and pyroptotic activities. In contrast to the above Cys modifications that inhibit pyroptosis, reactive oxygen species (ROS) was shown to potentiate pyroptosis and this process was dependent on Cys192 in mGSDMD (37). In fact, ~23% mGSDMD was reported to be oxidized at Cys192 in immortalized bone marrow–derived macrophages (iBMDMs) (37). Whether other posttranslational modifications target Cys191/192 in hGSDMD/mGSDMD in a similar manner as the *S*-palmitoylation of GSDME and how such modifications may regulate pyroptosis during inflammasome activation remain largely unexplored.

S-palmitoylation of cysteine residues, catalyzed by a family of 23 zinc finger aspartate–histidine–histidine–cysteine (ZDHHC) protein acyltransferases (PATs) in mammals, is the most common lipid modification of membrane-associated proteins (41–47), among which are mammalian GSDME and bacterial gasdermins. Since GSDMD associates with membrane to assemble oligomeric pores (9–13) and the conserved Cys191/192 is clearly important for its pyroptosis function, we hypothesize that Cys191/192 may be palmitoylated which modulates GSDMD association with membrane. Here, we report that the conserved Cys191 in hGSDMD was indeed *S*-palmitoylated and this posttranslational modification promoted pyroptosis. Mutation of Cys191 or treatment with palmitoyltransferase inhibitors cyano-myracrylamide (CMA) (48) or 2-bromopalmitate (2BP) (49) suppressed GSDMD localization to the membrane and dampened pyroptotic cell death or IL-1β secretion. In agreement, coexpression of GSDMD with palmitoyltransferases enhanced pyroptotic cell death, and exogenous palmitoylation sequences could fully restore pyroptotic activities to the C191A mutant. By contrast, GSDMD expression or cleavage was not affected by palmitoylation. Perhaps not surprisingly, *S*-palmitoylation was similarly observed for gasdermins from bacteria, fungi, invertebrates (34, 50–52) as well as mammals (33), suggesting that palmitoylation may be a shared regulatory mechanism for membrane translocation by this family of pore-forming proteins.

Results

Inhibition of Palmitoylation Suppresses GSDMD-Mediated Pyroptosis. *S*-palmitoylation is a common reversible modification of cysteines in membrane-associated proteins (41–46), among which are mammalian GSDME and bacterial gasdermins. Since the conserved Cys191 in hGSDMD and Cys192 in mGSDMD have been reported to contribute to their pyroptosis activities, we hypothesized that these cysteines may be palmitoylated which modulates the function of GSDMD. To first analyze whether GSDMD-mediated pyroptosis is affected by palmitoylation, phorbol-12-myristate-13-acetate (PMA) differentiated THP-1 cells were treated with lipopolysaccharides (LPS) followed by nigericin to stimulate the NLRP3 inflammasome and GSDMD-mediated pyroptosis (4–6). The cells were treated in the absence or presence of a specific palmitoyltransferase inhibitor CMA (48) to probe its effects on pyroptosis, namely, lactate dehydrogenase (LDH) release, as well as IL-1β secretion. Interestingly, CMA suppressed LDH release (Fig. 1*A*) and IL-1β secretion (Fig. 1*B*) in a time-dependent manner, suggesting that inhibition of palmitoylation negatively regulates the process of pyroptosis and cytokine secretion. This was corroborated with treatment using another inhibitor of palmitoyltransferases 2BP, which also diminished LDH release (Fig. 1*A*) and IL-1β secretion (Fig. 1*B*). Similarly, propidium iodide (PI) uptake, a measurement of compromised plasma membrane integrity, was also suppressed (Fig. 1*C*). The effects of palmitoyltransferase inhibitors were dose-dependent. Treatment with increasing concentrations of 2BP in both THP-1 cells and mouse iBMDMs demonstrated a dose-dependent suppression of LDH release and IL-1β secretion (*SI Appendix*, Fig. S1 *A* and *B*), suggesting minimal toxicity from 2BP treatment at the time frame and concentration range used in our experiments. Our data thus suggest that inhibition of palmitoylation suppresses GSDMD-mediated pyroptosis and IL-1β secretion.

Palmitoylation of hGSDMD-NTD Contributes to Pyroptosis. To probe the potential palmitoylation of GSDMD, we employed an acyl-biotin exchange (ABE) assay (53, 54), a well-established method in which hydroxylamine (HAM) hydrolyzes the labile thioester bonds between acyl chains and Cys residues, leaving free sulfhydryl groups that can be subsequently labeled with biotin and enriched with streptavidin agarose. Using the THP-1 cells stimulated with LPS and nigericin mentioned above, we first employed the ABE assay to probe the palmitoylation of endogenous GSDMD. Endogenous GSDMD was palmitoylated upon LPS treatment, which was elevated upon NLRP3 activation through nigericin treatment (Fig. 2*A*). This was significantly suppressed by 2BP treatment, and correlates with our observation that inhibition of palmitoylation negatively regulates pyroptosis and cytokine secretion (Fig. 1 *A* and *B*). Our data thus suggest that palmitoylation of GSDMD may contribute to its pyroptosis

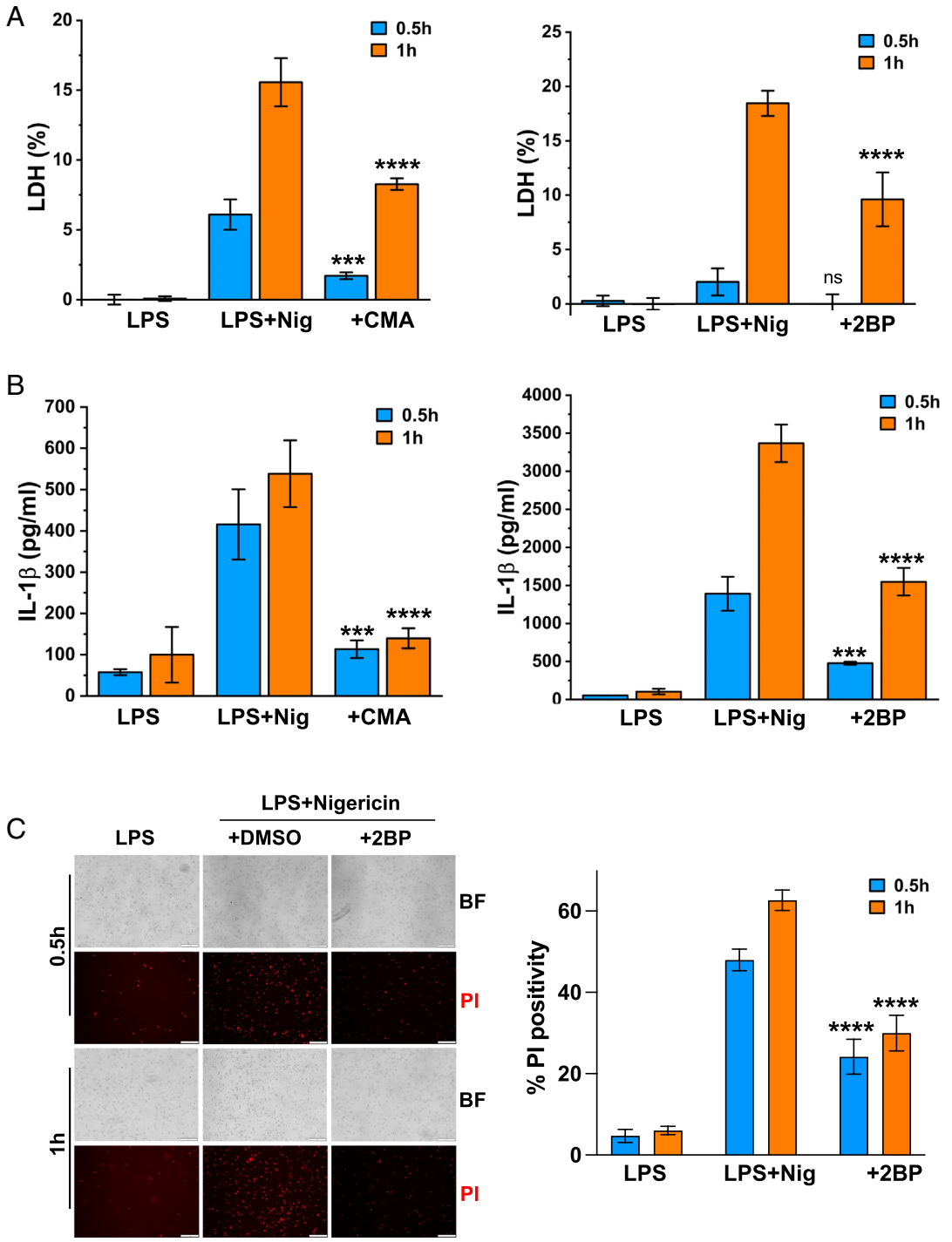

Fig. 1. Inhibition of palmitoylation suppresses GSDMD-mediated pyroptosis and cytokine release. (*A*) PMA differentiated THP-1 cells were treated with 1 μg/mL LPS for 4 h followed by 20 μM nigericin in the presence or absence of 100 μM CMA or 2BP. LDH release was measured at 0.5 or 1 h after nigericin treatment. (*B*) THP-1 cells were treated as in (*A*). IL-1β secretion was measured after nigericin treatment. (*C*) THP-1 cells treated in (*A*) were stained with propidium iodide after 0.5 or 1 h of nigericin treatment. "BF" denotes bright-field and "PI" denotes staining with propidium iodide. (Scale bars, 200 μm.) Quantitation of the PI-positive cells is shown on the right. Data are plotted as mean ± SD from at least three independent experiments. Statistical analyses were performed using two-way ANOVA with Bonferroni's multiple comparisons test versus the "LPS+Nig" samples. **P* < 0.05, ***P* <0.01, ****P* < 0.001, *****P* < 0.0001. See also *SI Appendix*, Fig. S1.

activities. Notably, the levels of GSDMD expression or cleavage was not affected by 2BP treatment (Fig. 2*A*), suggesting that palmitoylation of GSDMD may instead impact downstream events such as GSDMD pore formation in the membrane.

GSDMD contains an NTD and a CTD connected by a flexible linker. To investigate which domain of GSDMD is palmitoylated, ABE assays were performed with HEK293T cells expressing the full-length or NTD/CTD of hGSDMD. Both the full-length and the NTD of hGSDMD were palmitoylated (Fig. 2*B*), whereas the CTD was not (*SI Appendix*, Fig. S2*A*) even though it contains five Cys residues. As was observed in THP-1 cells, GSDMD palmitoylation was suppressed by 2BP treatment (Fig. 2*B*), which correlates with dampened LDH release from HEK293T cells transiently expressing hGSDMD-NTD (Fig. 2*C*). Using a tetracycline-inducible expression system in HEK293T cells, which was more amenable to tracking the time course of pyroptosis upon induction of hGSDMD-NTD expression, we observed that LDH release was suppressed upon 2BP treatment in a time-dependent manner

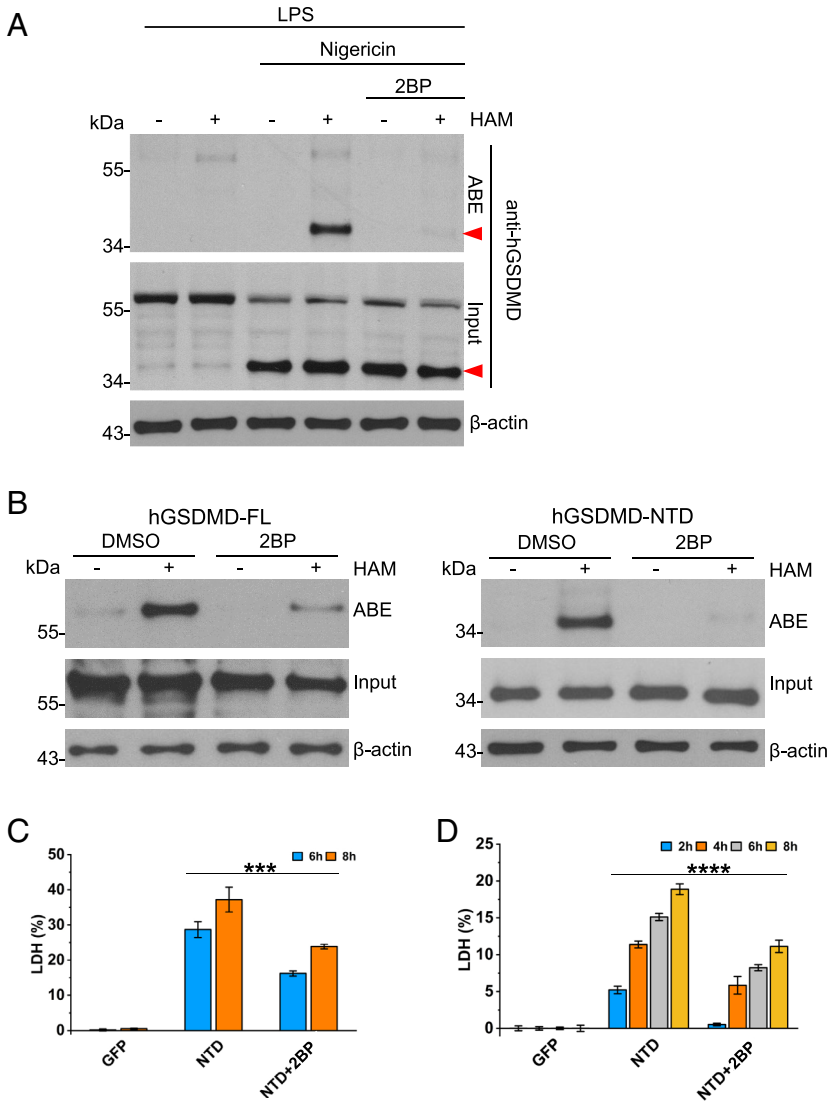

Fig. 2. *S*-palmitoylation of GSDMD in THP-1 and HEK293T cells. (*A*) PMA differentiated THP-1 cells were treated with LPS and nigericin, in the presence or absence of 100 μM 2BP. After 1 h of nigericin treatment, ABE assays were performed and GSDMD was probed with anti-hGSDMD antibody. The red arrows mark the hGSDMD-NTD. (*B*) FLAG-tagged full-length ("FL," *Left* panel) and N-terminal domain ("NTD," *Right* panel) from human GSDMD expressed in HEK293T cells were subjected to ABE assays, in the absence or presence of 100 μM 2BP. (*C*) LDH release from HEK293T cells transiently expressing hGSDMD-NTD in the presence or absence of 2BP was analyzed at 6 or 8 h posttransfection. (*D*) LDH release from HEK293T cells expressing hGSDMD-NTD in a tetracycline-inducible system was analyzed 2, 4, 6, or 8 h following tetracycline induction. Data are plotted as mean ± SD from at least three independent experiments. Statistical analyses were performed using two-way ANOVA with Bonferroni's multiple comparisons versus the NTD samples. *P < 0.05, **P < 0.01, ***P < 0.001, ****P < 0.0001. See also *SI Appendix,* Fig. S2.

(Fig. 2*D*). This is consistent with the delayed pyroptosis observed in the transient expression system (Fig. 2*C*) and in THP-1 cells (Fig. 1*A*). In agreement, propidium iodide (PI) uptake upon hGSDMD-NTD expression was also dampened by 2BP treatment (*SI Appendix*, Fig. S2*B*). Collectively, our data suggest that palmitoylation of hGSDMD-NTD contributes to pyroptosis. Interestingly, ABE assays also demonstrated that the full-length (*SI Appendix*, Fig. S2*C*) and NTDs (*SI Appendix*, Fig. S2*D*) from other gasdermin family members may also be palmitoylated, suggesting a shared mechanism of posttranslational modification for the gasdermin family members.

hGSDMD Is Palmitoylated at Cys191. As our data from both THP-1 and HEK293T cells suggest that GSDMD-mediated pyroptosis is regulated by palmitoylation and the NTD of hGSDMD may be palmitoylated, we turned our attention to potential *S*-palmitoylation site(s) among the three Cys residues (Cys38, Cys56, Cys191) in hGSDMD-NTD. To determine the palmitoylation site(s), point mutation of the Cys residues was introduced followed by ABE assays. Palmitoylation of hGSDMD-NTD was significantly reduced when Cys191 was mutated to Ala, in contrast to mutations of the other two Cys residues (Fig. 3*A*). In agreement, the C191A mutant exhibited much delayed lytic cell death as the time course of LDH release was monitored using the tetracycline-inducible expression system, compared with the C38A and C56A mutants that were indistinguishable from the wildtype (Fig. 3*B* and *SI Appendix*, Fig. S3*A*). The delayed kinetics of lytic cell death by the C191A mutant was similarly observed using the transient expression system (*SI Appendix*, Fig. S3*B*). Our data thus suggest that Cys191 of hGSDMD is palmitoylated and contributes to pyroptosis.

Many membrane-associated proteins contain signature sequences harboring known palmitoylated Cys residues. Some examples of these are 10 to 15 residue sequences from the N terminus of human growth-associated protein-43 (GAP43) (55), or the C termini of yeast amino acid transporters GAP1 and

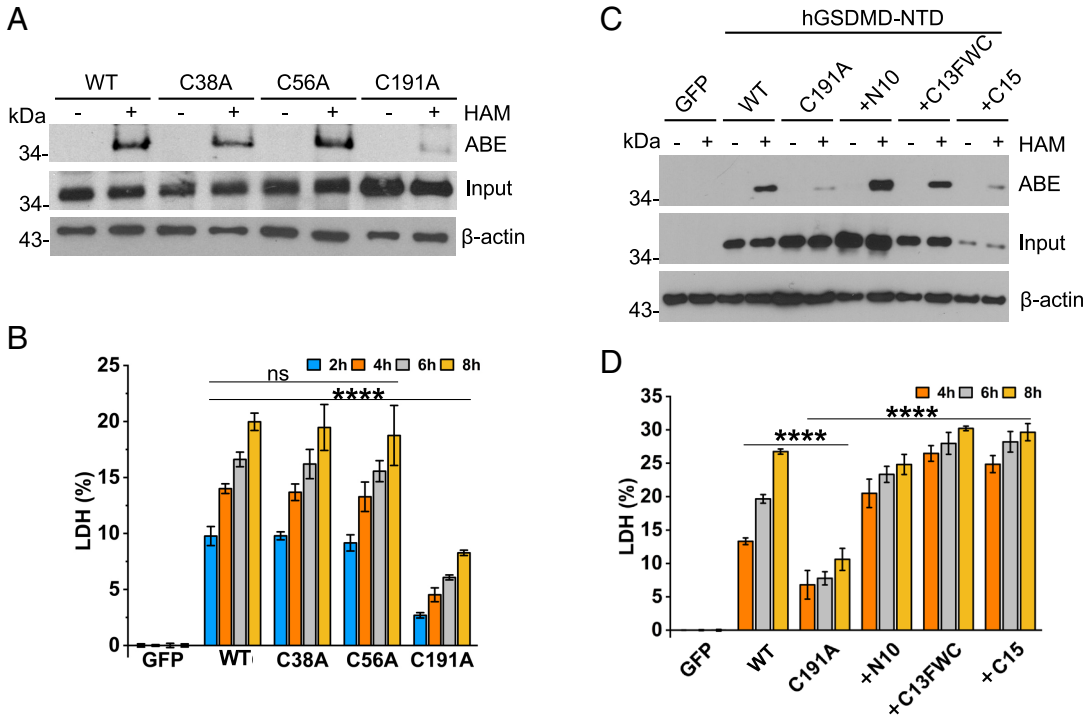

Fig. 3. Cysteine 191 of hGSDMD is palmitoylated. (*A*) The wildtype hGSDMD-NTD (denoted "WT") or C38A, C56A, and C191A mutants were expressed in HEK293T cells and ABE assays were performed to probe potential palmitoylation. (*B*) Time course of LDH release from cells in (*A*) expressing the wildtype or mutant hGSDMD-NTDs. (*C*) ABE assays were performed with HEK293T cells expressing hGSDMD-NTD in the wildtype form, C191A mutant form, and the C191A mutant chimera forms containing palmitoylation sequences at the N or C terminus of hGSDMD-NTD. The exogenous palmitoylation sequences are as follows: N10 is from the N terminus of human GAP43 protein with the sequence MLCCMRRTKQ; C13FWC is from the C terminus of yeast CAN1 protein with the sequence DHEPKTFWDKFWNFWC; C15 is from the C terminus of yeast GAP1 protein with the sequence MATKPRWYRIWNFWC. (*D*) Time course of LDH release from cells in (*C*) expressing the wildtype or C191A mutant hGSDMD-NTD, or mutant chimeras harboring the exogenous palmitoylation sequences. Data are plotted as mean ± SD from at least three independent experiments. Statistical analyses were performed using two-way ANOVA with Bonferroni's multiple comparisons versus the WT or "C191A" samples. **P* < 0.05, ***P* < 0.01, ****P* < 0.001, *****P* < 0.0001, ns: not significant. See also *SI Appendix*, Fig. S3.

CAN1 (56). To investigate whether these sequences could compensate for the loss of palmitoylation in the C191A mutant, we introduced them at the N or C terminus of the C191A mutant to generate chimera hGSDMD-NTDs. Interestingly, despite the different palmitoylation sequences from human and yeast proteins, and the location of these sequences at the N or C terminus rather than at an internal loop as Cys191, these sequences restored palmitoylation to the chimeras (Fig. 3*C*). Furthermore, the chimeras were able to induce LDH release to levels comparable to that by the wildtype hGSDMD-NTD (Fig. 3*D*). Our data thus demonstrate that exogenous palmitoylation sequences at different locations of hGSDMD-NTD can compensate for the loss of palmitoylation at Cys191 and pyroptosis by the C191A mutant, suggesting that the C191A mutant harbors no other defects except for the loss of palmitoylation. This further supports the importance of palmitoylation for GSDMD-mediated pyroptosis.

Cys191 Palmitoylation Regulates Membrane Localization of hGSDMD. Palmitoylation is known to modulate trafficking of integral and peripheral membrane proteins (41–46). As palmitoylation did not affect the levels of GSDMD expression or its cleavage (Fig. 2*A*), we investigated whether palmitoylation may regulate GSDMD membrane localization. Subcellular fractionation was performed for HEK293T cells expressing the wildtype or the C191A mutant hGSDMD-NTD. The wildtype hGSDMD-NTD was located predominately in the membrane fraction with trace amount in the cytosolic fraction (Fig. 4*A*). By contrast, treatment with 2BP led to a significant portion of hGSDMD-NTD being retained in the cytosolic fraction (Fig. 4*A*). The C191A mutant displayed a distribution pattern of hGSDMD-NTD similar to that of the 2BP-treated sample (Fig. 4*A*), suggesting that absence or inhibition of palmitoylation shifted the distribution of GSDMD away from the membrane. In agreement, imaging of cells expressing GFP-tagged hGSDMD-NTD revealed that the wildtype protein was primarily located at the cell surface, whereas both 2BP-treated or C191A mutant of hGSDMD-NTD were retained primarily in the cytosol (Fig. 4*B*). Furthermore, subcellular fractionation of the hGSDMD-NTD chimeras mentioned above revealed dominant localization of the chimeras in the membrane fraction (*SI Appendix*, Fig. S3*C*), similar to the wildtype protein and correlated with the palmitoylation and LDH release data. Collectively, these findings highlight the role of palmitoylation in regulating the localization of hGSDMD-NTD at the membrane, which may impact its ability to assemble membrane pores and induce pyroptosis.

ZDHHC7 Palmitoylates GSDMD and Promotes Pyroptosis. Palmitoylation is catalyzed by a family of 23 palmitoyl S-acyltransferase ZDHHCs, and these enzymes often harbor overlapping substrate specificities (41–46). To probe which ZDHHC PATs are responsible for the palmitoylation of hGSDMD, we first examined the expression levels of ZDHHC proteins in LPS-primed THP-1 cells through quantitative RT-qPCR as reported (57). The normalized RT-qPCR data showed that ZDHHC4, 5, 6, 7, 9, 11, 16, and 20 were expressed at relatively high levels compared with other ZDHHCs (*SI Appendix*, Fig. S4*A*). As expression of the wildtype hGSDMD-NTD led to high levels of LDH release within a short period of time (Fig. 2), we looked for a hGSDMD-NTD mutant that harbors reduced pyroptosis activity to allow the effects of ZDHHCs to be observable within a reasonable timeframe when they were coexpressed with hGSDMD-NTD. Our previous work on the full-length GSDMD (38) and the published GSDMD pore structure (15) revealed the

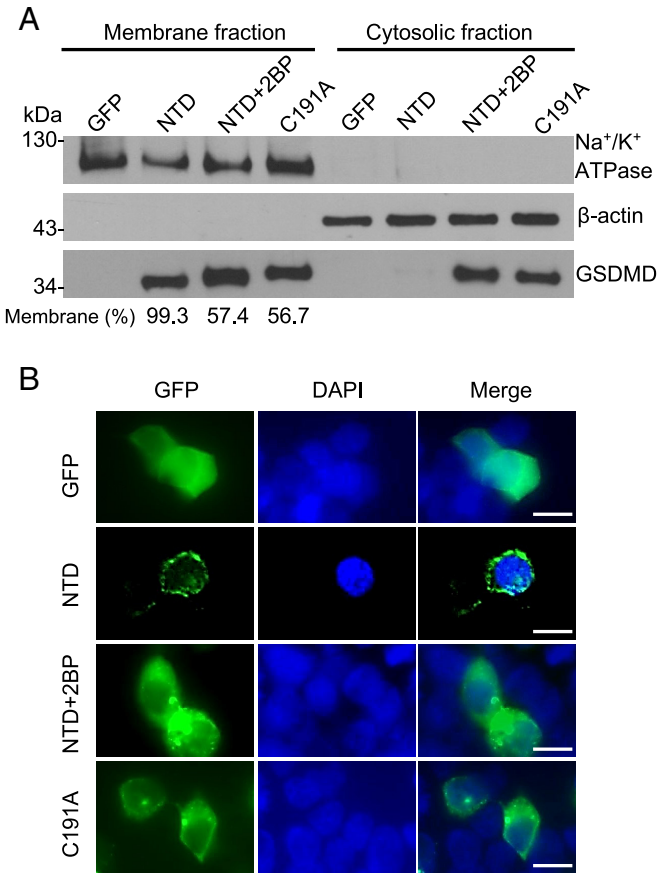

Fig. 4. Palmitoylation of hGSDMD facilitates its localization to the plasma membrane. (*A*) Analysis of the membrane or cytosolic fractions of HEK293T cells expressing the wildtype or C191A mutant of hGSDMD-NTD. The percentage of GSDMD in the membrane fractions for the NTD, NTD+2BP, and C191A samples is marked. (*B*) Subcellular localization of GFP-tagged wildtype or C191A mutant of hGSDMD-NTD with or without 2BP treatment. (Scale bars, 5 μm.)

importance of the α1 helix in both membrane lipid binding and oligomerization. We then found that an F5A mutant, located at the α1 helix of GSDMD, harbors impaired pyroptosis function as shown in Fig. 5, perhaps due to its reduced lipid-binding and/or oligomerization ability. Using this hGSDMD-NTD mutant, coexpression of ZDHHCs led to increased pyroptosis as assayed through LDH release, with ZDHHC7 demonstrating the highest level of enhancement (Fig. 5*A*). In agreement, palmitoylation of hGSDMD-NTD was elevated the most upon coexpression with ZDHHC7 (Fig. 5*B*). Similarly, coexpression of ZDHHC7 with the murine GSDMD-NTD F5A mutant led to increased pyroptosis and mGSDMD-NTD palmitoylation (Fig. 5 *C* and *D*). Collectively, these data suggest that ZDHHC7 can catalyze palmitoylation of hGSDMD-NTD and mGSDMD-NTD, which facilitates pyroptosis.

Inhibition of Palmitoylation Alleviates *Gsdmd*-Dependent Inflammatory Tissue Damage and Death. To probe the role of palmitoylation in regulating GSDMD function in vivo, intraperitoneal (i.p.) LPS injection was performed with 6- to 8-wk-old age- and sex-matched C57BL6/J mice (~20 g each). Prior to LPS injection, mice were pretreated with 2BP (20 or 50 mg/kg, i.p.). Pretreatment with 2BP increased the survival of LPS-injected mice in a dose-dependent manner as a higher amount of 2BP treatment led to increased survival (Fig. 6*A*), in agreement with the dose-dependent suppression of pyroptosis observed in macrophages (*SI Appendix*, Fig. S1). Importantly, injection of LPS in *Gsdmd* deficient mice did not affect survival, consistent with previous reports that the LPS-induced death in mice was primarily dependent on *Gsdmd* (4–6). Furthermore, treatment of mice with 2BP alone did not lead to death of the animals for up to 8 d, suggesting minimal toxicity for the dosage used here (Fig. 6*A*). In agreement with the survival data, severe lung tissue damage was observed in LPS-treated WT mice, with intra-alveolar edema, mixed inflammatory infiltrates, and mildly thickened bronchial walls (Fig. 6*B*). Pretreatment with low dose 2BP improved LPS-induced lung damage with visible alveolar hemorrhage and lymphocytic infiltration (Fig. 6*B*), while high dose 2BP largely restored alveolar structure with only scattered lymphocytic infiltrates (Fig. 6*B*). In contrast to the WT mice, *Gsdmd*$^{-/-}$ mice were largely protected from LPS-induced lung injury with moderate alveolar damage and interstitial inflammation (Fig. 6*B*), while alveolar structure was generally normal/preserved with high dose 2BP (Fig. 6*B*). Control *Gsdmd*$^{-/-}$ mice administered 2BP only (Fig. 6*B*) showed normal lung histology with intact alveolar structures, similar to vehicle-treated mice. Consistent with the above observations, in WT mice injected with LPS, serum cytokine levels for IL-1β, IL-18, IL-6, IL-12p70, TNF, GM-CSF, IFNγ, and IL-2 were significantly elevated and were dose-dependently reduced upon 2BP treatment (Fig. 6*C*). By contrast, the serum cytokine levels for the *Gsdmd*$^{-/-}$ mice injected with LPS showed minimal or no increase. Taken together, our data suggest that *Gsdmd*-dependent inflammatory tissue damage and death are alleviated by palmitoylation inhibition in vivo.

Discussion

Gasdermin-mediated pyroptosis plays important roles in inflammation and host defense. The regulatory mechanisms for pore-formation and pyroptosis by gasdermins remain incompletely understood. Here, we report that a conserved Cys191 residue in hGSDMD was *S*-palmitoylated and this posttranslational modification was important for hGSDMD localization to the membrane, which promoted pyroptosis and cytokine release. Mutation of Cys191 or treatment with palmitoyltransferase inhibitors such as CMA or 2BP suppressed hGSDMD membrane localization, pyroptotic cell death, or IL-1β secretion, without apparent impact on GSDMD cleavage. By contrast, coexpression of hGSDMD with palmitoyltransferases enhanced pyroptotic cell death. Our data thus suggest that pyroptosis is facilitated by palmitoylation. Furthermore, addition of exogenous palmitoylation sequences at different locations of hGSDMD-NTD was fully capable of rescuing palmitoylation and pyroptotic activities of the C191A mutant. This demonstrates that the loss of palmitoylation at Cys191 can be fully compensated for by the exogenous palmitoylation sequences, and the C191A mutant harbors no other defects except for the loss of palmitoylation. In other words, palmitoylation-mediated membrane localization may be distinct from other molecular events such as GSDMD cleavage or conformational change during pore assembly. Collectively, our data support a model in which palmitoylation at Cys191 facilitates membrane localization of GSDMD, which promotes pyroptosis and cytokine release (Fig. 7).

Despite intensive studies, the molecular events underlying the transition of GSDMD from an autoinhibited soluble form to an oligomeric pore form inserted into the membrane remain incompletely understood. The *S*-palmitoylation-facilitated membrane localization described here may be distinct from other events in GSDMD-mediated pyroptosis: *S*-palmitoylation of Cys191 may facilitate membrane localization of hGSDMD that promotes pore assembly, whereas the conformational change of hGSDMD per se may still proceed in the absence of palmitoylation, albeit with

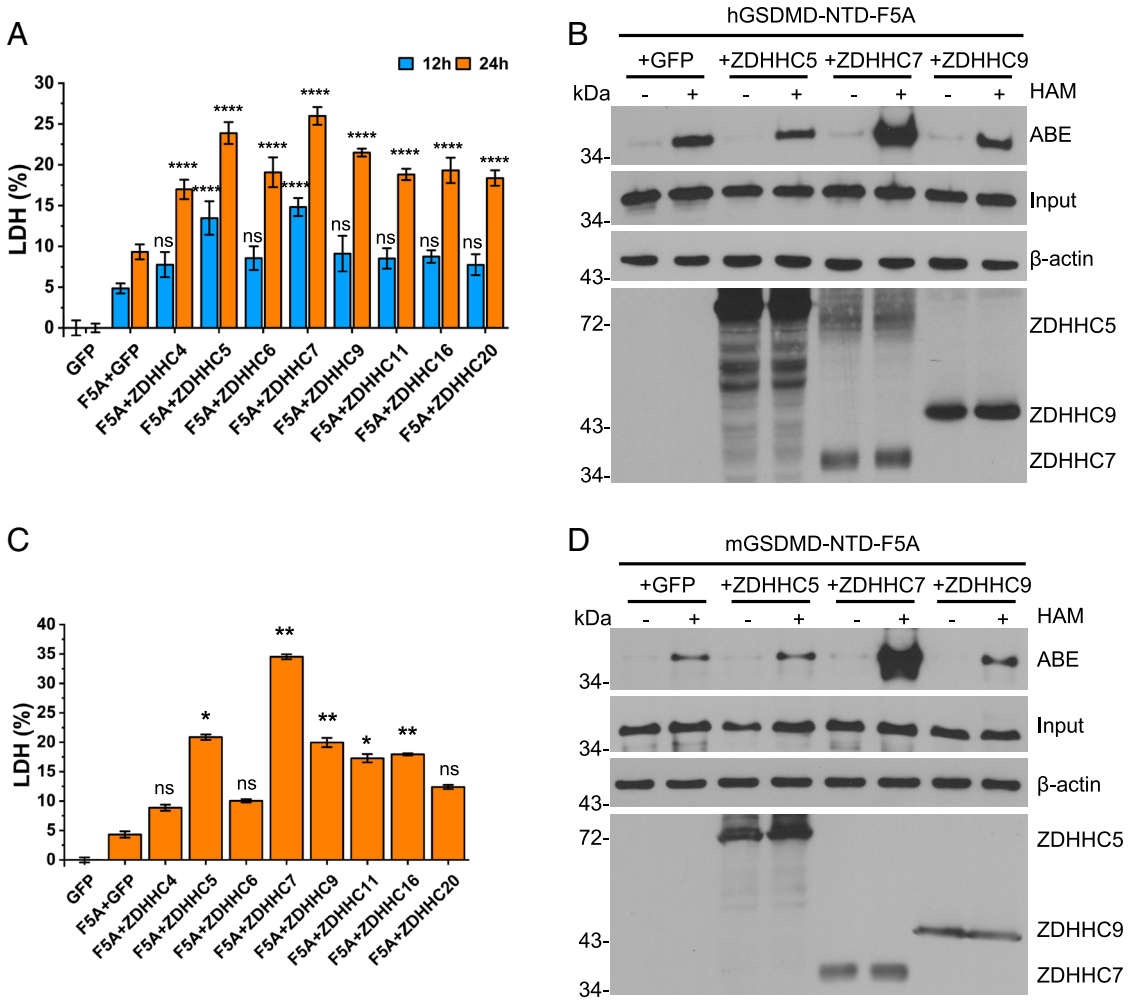

Fig. 5. ZDHHC palmitoyltransferases catalyze the palmitoylation of hGSDMD and mGSDMD. (*A*) LDH release from HEK293T cells expressing the F5A mutant of hGSDMD-NTD along with various ZDHHC palmitoyltransferases, 12 or 24 h posttransfection. (*B*) ABE assays were performed for HEK293T cells coexpressing hGSDMD-NTD F5A mutant and ZDHHC5, 7, or 9 enzymes, 24 h posttransfection. (*C*) LDH release from HEK293T cells expressing the F5A mutant of mGSDMD-NTD along with various ZDHHC palmitoyltransferases, 24 h posttransfection. (*D*) ABE assays were performed for HEK293T cells coexpressing mGSDMD-NTD F5A mutant and ZDHHC5, 7, or 9 enzymes, 24 h posttransfection. Data are plotted as mean ± SD from at least three independent experiments. Statistical analyses were performed using two-way (*A*) or one-way (*C*) ANOVA with Bonferroni's multiple comparisons test versus the "F5A+GFP" samples. **P* < 0.05, ***P* < 0.01, ****P* < 0.001, *****P* < 0.0001, ns: not significant. See also *SI Appendix,* Fig. S4.

much diminished efficiency of pore formation in light of the delayed pyroptosis with the C191A mutant. Notably, a recent report further suggested that palmitoylation of GSDMD promoted both membrane localization and oligomerization (58). In the current study, when pyroptosis was monitored in a time course, inhibition of palmitoylation or the C191A mutation delayed hGSDMD-mediated pyroptosis but did not completely abrogate it. In agreement, Johnson and colleagues recently reported that for several bacterial gasdermins, membrane insertion of palmitoyl moiety is critical for efficient pore formation (34, 59). Although deficiency in *S*-palmitoylation did not completely abrogate GSDMD-mediated pyroptosis, modulating the efficiency of gasdermin pore formation through palmitoylation may have important physiological consequences in vivo. For example, this may allow time for membrane repair mediated by the endosomal sorting complexes required for transport (ESCRT) machinery (60) or caspase-7-activated acid sphingomyelinase (ASM) (61), thus alleviating or reversing certain inflammatory process involving pyroptosis.

S-palmitoylation, first observed in viral glycoproteins (62), is the most common lipid modification of proteins that regulates protein stability, trafficking, membrane localization, and interaction with lipids or other proteins (41–46). It has been reported for diverse proteins such as small GTPase Ras (63), innate immune receptor or signaling molecules NLRP3 (64), NOD1/2 (65) or STING (66), and the SARS-CoV-2 spike protein (67–69). *S*-palmitoylation bears similarity to phosphorylation, is dynamic, and reversible, due to the labile thioester linkage that is catalyzed by a family of 23 palmitoyl S-acyltransferase ZDHHCs, which are membrane proteins themselves and therefore may have ready access to substrates within or near the membrane (41–46). As a result, it is possible that membrane localization and palmitoylation of substrates by ZDHHCs may mutually enhance each other. Here, we identified ZDHHC7 as the primary enzyme that palmitoylates hGSDMD and mGSDMD to regulate their pyroptotic activities in HEK293T cells. While this manuscript was in preparation, three reports suggested that GSDMD is palmitoylated in macrophages by several ZDHHCs including ZDHHC5, 7, and 9, which regulates pyroptosis (58, 70, 71). Given the broad substrate specificities and inherent redundancies of ZDHHC enzymes (72, 73), it is perhaps not surprising that there are overlapping specificities among different ZDHHCs for GSDMD palmitoylation under different stimulation conditions in different cells or tissues. Our study and others thus advance our understanding of gasdermin regulation by a different family of

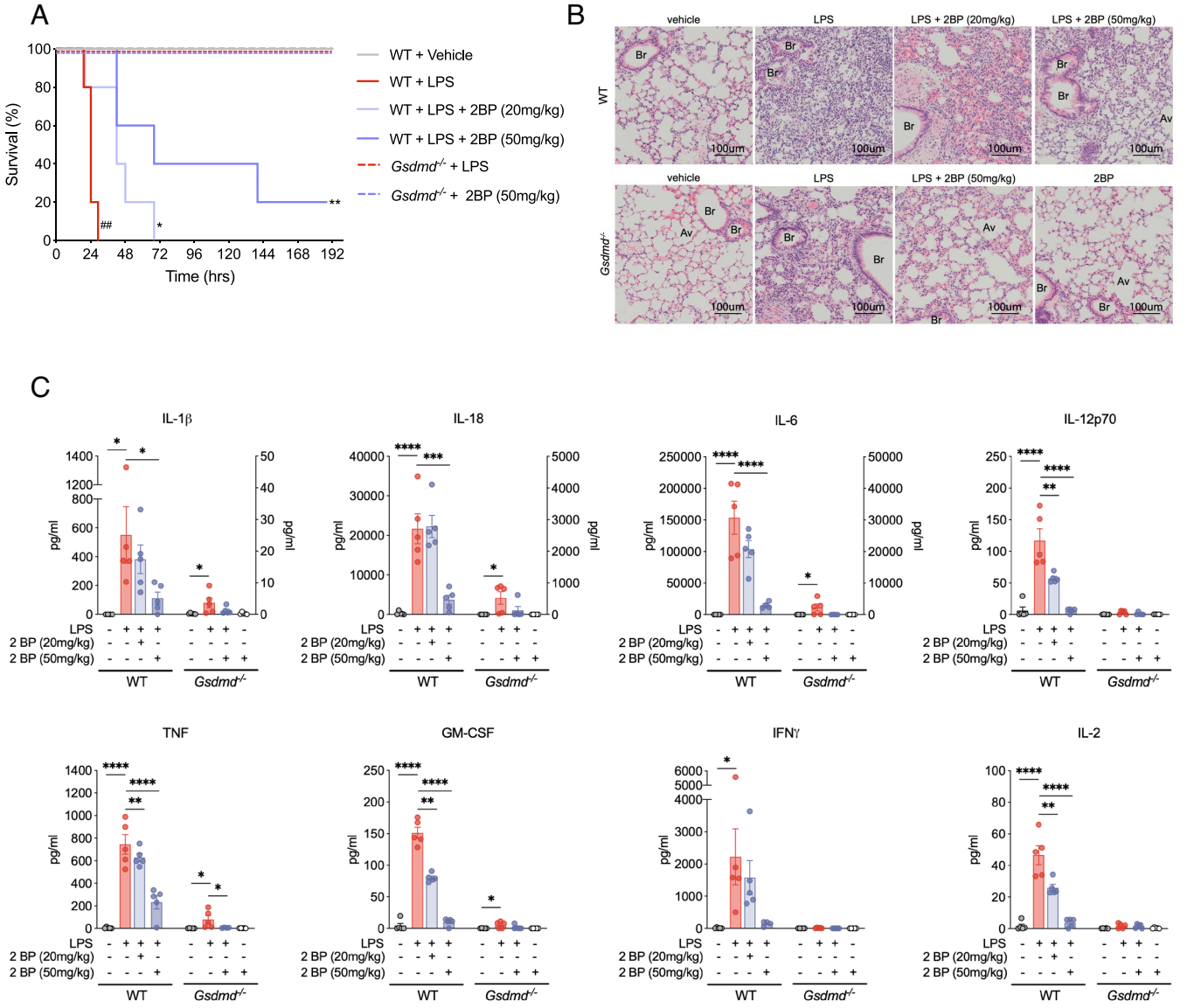

Fig. 6. Inhibition of palmitoylation mitigates inflammation and death of LPS-injected mice. (*A*) C57BL6/J (WT) and *Gsdmd*$^{-/-}$ mice were pretreated with 2BP or vehicle, and challenged 4 h later with LPS or vehicle. After administration of LPS/vehicle, survival was monitored twice daily for 5 d (120 h) and once daily for remaining 3 d. The Kaplan–Meier survival curve is representative of 4 to 5 experiments ($n \geq 3$/experiment); $^{\#\#}P < 0.01$ vs. vehicle, $^{*}P < 0.05$, $^{**}P < 0.01$ vs. LPS alone by log-rank (Mantel-Cox) test. (*B*) In separate experiments, mice were killed 12 h after LPS/vehicle, and the representative histologic images of H&E-stained lungs are shown. Severely damaged alveoli with intra-alveolar edema, mixed inflammatory infiltrates consisting of neutrophils, lymphocytes, macrophages, occasional plasma cells, and mildly thickened bronchial walls were observed in WT mice treated with LPS (*Upper, Middle Left* panel). Pretreatment with low dose 2BP improved LPS-induced lung damage, but alveolar hemorrhage with red blood cells and lymphocytic infiltration occupying alveolar spaces/interstitial tissues were still evident (*Upper, Middle Right* panel), while high dose 2BP had a dramatic effect, largely restoring alveolar structure with only scattered lymphocytic infiltrates (*Upper, Far Right* panel). In contrast to the WT mice, *Gsdmd*$^{-/-}$ mice were largely protected from LPS-induced lung injury, but showed moderate alveolar damage with interstitial inflammation (*Lower, Middle Left* panel), while alveolar structure was generally normal/preserved with high dose 2BP (*Lower, Middle Right* panel). Control *Gsdmd*$^{-/-}$ mice administered 2BP only (*Lower, Far Right* panel) and vehicle-treated mice (*Upper/Lower, Far Left* panels) showed normal lung histology with intact alveolar structures. Original mag: X20 ($n = 5$); Av, alveolar space; Br, bronchiole. (*C*) Serum cytokine levels were measured 12 h after LPS/vehicle treatment and plotted for WT and *Gsdmd*$^{-/-}$ or *Gsdmd*$^{-/-}$ only on either *Left* or *Right* (when present) *y* axes, respectively. Data presented as mean ± SEM ($n = 5$); $^{*}P < 0.05$, $^{**}P < 0.01$, $^{***}P < 0.001$, $^{****}P < 0.0001$ by post hoc multiple comparisons using Šídák's test following significant ($P < 0.05$) one-way ANOVA.

enzymes, the ZDHHC palmitoyltransferases, in addition to the other known enzymes involved in posttranslational modifications of gasdermins through protease processing (4–6, 74, 75) or ubiquitination (31, 32, 76–78). The selective palmitoylation of Cys191/192 in GSDMD by ZDHHC enzymes suggests potential avenues for therapeutically targeting palmitoyltransferases catalyzing *S*-palmitoylation of GSDMD in inflammatory disorders.

It is currently unclear how GSDMD palmitoylation is regulated. Conceivably, diverse inflammatory signaling pathways may modulate the expression or enzymatic activities of the ZDHHC enzymes, regulate the location of the enzymes among the ER, Golgi, plasma membrane, and other membrane structures, impact the colocalization of ZDHHC and GSDMD, etc. We demonstrated that GSDMD was palmitoylated upon LPS treatment of macrophages, and nigericin treatment further augmented the total amount of palmitoylated GSDMD. This is consistent with similar observations by recent publications, which reported upregulation of ZDHHC enzymes upon LPS stimulation of macrophages (58). The reported different levels of GSDMD palmitoylation using different concentrations of LPS further suggests potential regulatory mechanism for inflammatory responses to various stimulations. Furthermore, GSDMD palmitoylation was reported to be augmented by ROS (58, 70), in agreement

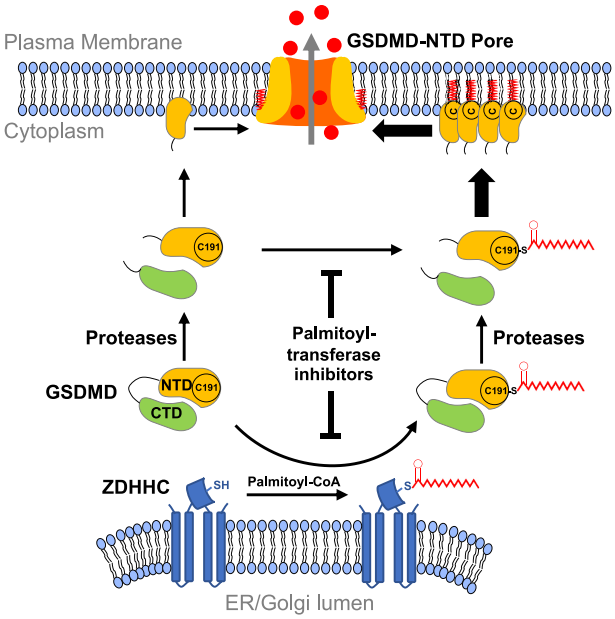

Fig. 7. Palmitoylation facilitates GSDMD-mediated pore formation and release of inflammatory cytokines. A model of how palmitoylation facilitates GSDMD-NTD localization to the membrane, thus promoting pyroptosis and cytokine release.

with the observation that GSDMD association with membranes was promoted by mitochondrial ROS (79). Another previous publication employing quantitative mass spectrometry to analyze murine GSDMD-NTD expressed in macrophages demonstrated that different fractions of multiple Cys residues were oxidized (37), ranging from 1.1% to 22.9%, including Cys192, Cys265, Cys57, and Cys77. Cys192 in mGSDMD is the equivalence of Cys191 in hGSDMD and was oxidized at the highest level at 22.9%. ROS may affect palmitoylation through multiple mechanisms, for example, either through direct targeting any combination of the above Cys residues in GSDMD, or through regulating other proteins such as the ZDHHC enzymes. Notably, our experiments using extraneous palmitoylation sequences to rescue palmitoylation and pyroptotic activities of the C191A mutant do not exclude the potential roles of ROS, due to the presence of other Cys residues in hGSDMD and the introduced palmitoylation sequences. In fact, targeted chemical proteomic approaches such as acyl-resin assisted capture (acyl-RAC) have identified proteins undergoing *S*-palmitoylation alongside other cysteine oxidative modifications (44, 80), suggesting potential combinatorial posttranslational modifications at various cysteines. As a result, palmitoylation and other Cys modifications such as oxidation may work in concert to regulate the structure and function of pore-forming proteins such as gasdermins.

Even though the scope of this work is limited to the studies of GSDMD, our findings are consistent with previous reports of widespread *S*-palmitoylation of gasdermins from bacteria, fungi, and invertebrates (34, 50, 51, 59), as well as mammalian GSDME (33). Our preliminary study also suggests that other mammalian gasdermin family members GSDMA-GSDME may be *S*-palmitoylated. It is thus conceivable that this posttranslational modification may be a shared regulatory mechanism throughout evolution for proteins such as gasdermins that translocate between the cytosol and membrane compartments. These regulatory mechanisms now include stabilization of gasdermin structure, facilitation of NTD–CTD dissociation, and promotion of membrane localization. The mechanisms of how palmitoylation modulates the structure and function of gasdermins, how gasdermins are recognized by specific palmitoyltransferases, and how diverse signaling pathways converge on the regulation of palmitoylation of different gasdermins will be exciting future avenues of investigation.

Materials and Methods

Cell Lines. HEK-293T and THP-1 cells were purchased from ATCC (Monassas, VA). iBMDM cells are from Eicke Latz (81). HEK-293T cells and iBMDM cells were cultured in Dulbecco's Modified Eagle Medium (DMEM) (Gibco, Grand Island, NY) supplemented with 10% FBS (Gemini BioProducts, West Sacramento, CA) and 1% penicillin/streptomycin (Gibco). THP-1 cells were cultured in RPMI 1640 medium (Gibco) containing 10% FBS, 1% penicillin/streptomycin, and 50 μM 2-mercaptoethanol (Acros Organics, NJ).

Antibodies. Monoclonal anti-mouse GSDMD antibody (A-7, sc-393656) and monoclonal anti-β-actin antibody (sc-47778) were from Santa Cruz Biotechnology (Dallas, TX), monoclonal anti-Flag M2 antibody (F3165) was from Millipore Sigma (St Louis, MO), anti-human GSDMD monoclonal antibody (E8G3F, #97558) and anti-Na^+, K^+-ATPase antibody (#3010S) were from Cell Signaling Technology (Danvers, MA). All primary antibodies for western blot were used following the manufacturer's instructions. The secondary antibodies against mouse and rabbit IgG were purchased from Cell Signaling Technology (Danvers, MA) and used according to the manufacturer's instructions.

Cloning and Site-Directed Mutagenesis. Coding sequences for the full-length and NTD of human GSDMA, GSDMB, GSDMC, GSDMD, and GSDME as well as the mouse GSDMD were cloned into pcDNA4/TO or pEGFP vectors. All mutants were generated using the overlap extension PCR mutation method and confirmed by sequencing.

Expression of Gasdermins and Cytotoxicity Assay. THP-1 cells grown in RPMI 1640 medium supplemented with 10% FBS were plated in 6-well plates and treated overnight with 100 ng/mL phorbol 12-myristate 13-acetate (PMA) (Millipore Sigma, St. Louis, MO). THP-1 cells grown in RPMI medium and iBMDM cells grown in DMEM were primed with 1 μg/mL LPS (Millipore Sigma, St. Louis, MO) for 4 h before stimulating with 20 μM nigericin (Millipore Sigma, St. Louis, MO) to active the NLRP3 inflammasome. In some conditions, 100 μM 2BP or CMA was added to the media 45 min before adding 20 μM nigericin. LDH release from each well at different time points was measured using the cytotoxicity detection kit from Roche (Indianapolis, IN) following the manufacturer's instructions.

For transient transfection, HEK293T cells grown in DMEM plus 10% fetal bovine serum (FBS) were transfected with plasmids using calcium phosphate or polyethylenimine (PEI) max (Polysciences, Warrington, PA). For tetracycline-inducible expression, pcDNA6/TR vector encoding Tet repressor (Thermo Fisher Scientific, Waltham, MA) was stably transfected into HEK293T cells under the selection of 5 to 10 μg/mL blasticidin. Various pCDNA4/TO vectors encoding gasdermins were then transfected into these cells. After overnight culture of the transfected cells, expression of indicated protein was induced with 1 μg/mL tetracycline. For fractionation experiments of the chimeras, cells were treated with tetracycline for 24 h. For coexpression of the F5A mutant of GSDMD-NTD and ZDHHCs, expression plasmids encoding the F5A mutant and individual ZDHHC enzyme were transfected at a 1:1.5 (w:w) ratio. After overnight culture of the transfected cells, 2 μg/mL tetracycline was added to induce expression of GSDMD-NTD, and the culture supernatants were collected after 24 h to assay for LDH release using a cytotoxicity detection kit from Roche (Indianapolis, IN) following the manufacturer's instructions. The LDH release was expressed as a percentage of total LDH content upon 1% Triton X-100 treatment of the cells.

IL-1β Release Assay. To measure secreted IL-1β, enzyme-linked immunosorbent assay (ELISA) was performed with the collected culture supernatants mentioned above. THP-1 or iBMDM cells were primed with LPS (1 μg/mL) for 4 h, followed by treatment with DMSO, 100 μM 2BP, or CMA for 45 min before adding 20 μM nigericin to stimulate the NLRP3 inflammasome. After 30 min stimulation, IL-1β in the culture media was measured and quantified using human IL-1 beta/IL-1F2 QuantiGlo ELISA kit (QLB00B, R&D systems, Minneapolis, MN) and Mouse IL-1

beta/IL-1F2 DuoSet ELISA Kit (DY401, R&D systems, Minneapolis, MN) following the manufacturer's instructions.

Microscopy Imaging of Cell Lines. To examine cell morphology and propidium iodide uptake, brightfield and fluorescent images of cells in 6-well plates were captured using an Olympus IX73 inverted fluorescent microscope. HEK293T cells were plated in eight chamber slides (Lab-Tek, Nunc Inc. Naperville, IL), 6 h post-transfection with plasmids coding for GFP or GFP-tagged hGSDMD-NTD, with or without 100 μM 2BP treatment. Cells were washed once with 1×PBS, then fixed with a buffer containing 4% formaldehyde in PBS and incubated for 10 min at room temperature. The slides were washed twice with 1×PBS, then PBS plus 0.1% Triton X-100 was added to permeabilize for 5 min at room temperature. After washing with 1×PBS, the slides were mounted with ProLong Gold antifade reagent with DAPI (Thermo Fisher Scientific, Waltham, MA) and imaged with the Olympus IX73 inverted microscope.

ABE Assay. The ABE protocol was adapted from a previous protocol (53). Cells were lysed with lysis buffer containing 50 mM Triethanolamine (TEA) (Millipore Sigma, St. Louis, MO), pH 7.0, 150 mM NaCl, 4% SDS, 4 mM EDTA with freshly added protease inhibitor cocktail (Roche, Indianapolis, IN), 1,500 units/ml Benzonase (#70664-3, Novagen, Darmstadt, Germany), and 5 mM PMSF. Brief sonication was used to facilitate complete lysis and reduce viscosity. The protein samples were precipitated with chilled methanol: chloroform: water (400 μL: 150 μL: 300 μL per 100 μL protein samples; then washed twice with 1 mL methanol) and the resulting pellet was dissolved in a reaction buffer containing 50 mM TEA, pH 7.0, 150 mM NaCl, 4% SDS, and 4 mM EDTA. 400 μg total protein was treated with 10 mM neutralized TCEP for 30 min with rotation, subsequently 140 mM N-ethylmaleimide (NEM, Thermo Fisher Scientific, Waltham, MA) was added to cap the reduced cysteines for 3 h at room temperature with shaking. After a second round of methanol–chloroform–water precipitation, the protein pellet was resuspended in 60 μL reaction buffer and split into two 30 μL aliquots for the +/− hydroxylamine (NH_2OH, HAM) conditions: for the +HAM samples, 90 μL of 1 M neutralized HAM dissolved in 0.2% Triton X-100, 50 mM TEA, pH 7.0, 150 mM NaCl was added; for the control, the above solution without HAM was added. After 3 h of incubation at room temperature, proteins were methanol–chloroform–water precipitated for a third time. The protein samples were dissolved in the reaction buffer and incubated with 1 mM biotin HPDP (APExBio, Houston, TX) for 30 min. The protein samples were precipitated again and dissolved in 2% SDS, 50 mM Tris, pH 7.5, 150 mM NaCl, 5 mM EDTA, and diluted 1:10 with an immobilization buffer containing 0.5% Triton X-100, 50 mM Tris, pH 7.5, 150 mM NaCl, and 5 mM EDTA. The protein samples were incubated with 50 μL streptavidin agarose beads (Thermo Fisher Scientific, Waltham, MA) at 4 °C overnight. Then the beads were washed four times with 1% Triton X-100, 50 mM Tris, pH 7.5, 150 mM NaCl, and 5 mM EDTA. The beads were boiled at 95 °C for 10 min with 2×Laemmli buffer containing 2-mercaptoethanol and subjected to SDS-PAGE and/or western blotting analysis.

Subcellular Fractionation. HEK293T cells expressing GSDMD were harvested and washed with cold 1×PBS. After resuspension with cold 1×PBS containing a protease inhibitor cocktail (Roche, Indianapolis, IN), cells were lysed through sonication. Cell lysates were then centrifuged at 100,000×*g* for 30 min to obtain the membrane and cytosolic fractions. After washing with cold 1×PBS, cell membrane fraction was dissolved in a buffer containing 2% SDS, 50 mM Tris, pH 7.5, 150 mM NaCl, and 5 mM EDTA. The cytosolic fraction was precipitated using chilled methanol: chloroform: water (400 μL: 150 μL: 300 μL per 100 μL lysate). The pellet was washed twice with 1 mL methanol, and dissolved in a buffer containing 2% SDS, 50 mM Tris, pH 7.5, 150 mM NaCl, and 5 mM EDTA. The membrane and cytosolic fractions were subjected to SDS-PAGE and western blot.

qRT-PCR. qRT-PCR were performed with samples of THP-1 cells primed with LPS (1 μg/mL) for 4 h. Total RNA was isolated using the RNeasy Mini Kit (Qiagen, Hilden, Germany), and RNA was reverse transcribed to cDNA using iScript Reverse Transcription Supermix for RT-qPCR (Bio-Rad, Hercules, CA) following the manufacturer's standard protocol. qRT-PCR of samples was performed using primers for GAPDH (forward, 5′-GTCTCCTCTGACTTCAACAGCG-3′ and reverse, 5′-ACCACCCTGTTGCTGTAGCCAA-3′), and primers for ZDHHC enzymes described previously (57). qRT-PCR were performed with iQ SYBR Green Supermix (Bio-Rad, Hercules, CA) using a Bio-Rad CFX 96 real-time PCR detection system following the manufacturer's standard protocol. The gene expression level was normalized to that for GAPDH.

In Vivo Studies. Experiments were conducted in a blinded manner, with mice randomized to different interventions using a progressive numeric label, the code only known to animal caretakers and revealed at the end of each experiment. 6- to 8-wk-old age- and sex-matched C57BL/6 J-*Gsdmd*^{em1Vnce}/J (*Gsdmd*$^{-/-}$) (Strain #:032663, The Jackson Laboratory, Bar Harbor, ME) and WT mice were treated with 2BP (cat#238422, Sigma-Aldrich, St. Louis, MO) 4 h prior to administration of LPS (*Escherichia coli* O111:B4, cat #L2630, Sigma-Aldrich) and monitored for up to 8 d post-LPS injection. Briefly, lyophilized 2BP was reconstituted in DMSO and further diluted in PBS with probe sonication to increase solubility properties. Experimental mice (~20 g) were pretreated with either vehicle or 2BP (20 or 50 mg/kg, i.p.), and subsequently with either vehicle or LPS (25 mg/kg, i.p.). Mice were monitored for survival twice daily for first 5d and once daily for next 3d. In separate experiments using the aforementioned protocol, whole blood was collected 12 h after LPS/vehicle from anesthetized mice by cardiac puncture, with serum obtained after centrifugation at 15,000 rcf for 10 min at 4 °C and stored at −20 °C for later cytokine assay (see below). Experimental mice were then immediately killed and whole lungs removed for histological evaluation. All procedures were approved by the CWRU Institutional Animal Care and Use Committee and were in accordance with the Association for Assessment and Accreditation of Laboratory Animal Care guidelines.

Tissue Harvest and Cytokine Assays. Whole lung tissues were processed by the Histology/Imaging Core (Core C) of the Cleveland DDRCC (NIH P30 DK097948). Briefly, immediately after harvest, lungs were submerged in 4% PFA (ChemCruz Biotechnology, Inc., Dallas, TX), rinsed in 70% ethanol after 24 h, processed, paraffin-embedded, and sectioned at 3 to 4 μm. Specimens were stained with H&E and evaluated by a trained pathologist blinded to experimental groups. Cytokine levels were measured in serum from experimental mice by the Bioanalyte Core at CWRU. Specifically, serum samples were run in duplicate by Luminex xMAP technology using the ProcartaPlex™ Mouse Th1/Th2 Cytokine Panel, 11plex, according to the manufacturer's instructions (cat#EPX110-20820-901, Invitrogen, Thermo Fisher Scientific, Waltham, MA), and protein levels reported as pg/ml for each cytokine.

Quantification and Statistical Analysis. Statistical analyses were performed with program Excel (Microsoft Corporation, Redmond, WA), Origin (OriginLab, Northampton, MA), or GraphPad Prism (GraphPad Software, Boston, MA).

Data, Materials, and Software Availability. All study data are included in the article and/or *SI Appendix*.

ACKNOWLEDGMENTS. We thank Dr. Hongbo Luo, Dr. Paul Jenkins, and Dr. Masaki Fukata for the ZDHHC plasmids. We are grateful to Dr. Hongbo Luo and Dr. Arumugam Balasubramanian for advice on in vivo studies. We thank Joseph Williams for technical support for in vivo experiments. We thank Brianna M. Busscher for assistance with western blot. We thank the Xiao, Abbott, Dubyak, and Pizarro lab members for thoughtful discussions. This work has been supported in part by NIH Grants R01GM127609, R01AI143992, and P01AI141360 to T.S.X., R03AI173549 to Z.L., R35GM119840 to B.C.D., P01AI141360 to T.T.P., T32GM007250 and the Dr. Jerome Kleinerman Student Research Fellowship to S.B. We acknowledge histology support from the Histology/Imaging Core of the Cleveland DDRCC (NIH P30 DK097948).

Author affiliations: [a]Department of Pathology, Case Western Reserve University, Cleveland, OH 44106; [b]Ministry of Education Key Laboratory for Membraneless Organelles and Cellular Dynamics, Hefei National Research Center for Physical Sciences at the Microscale, Division of Life Sciences and Medicine, University of Science and Technology of China, Hefei, Anhui 230027, China; [c]Proteomics and Metabolic Core, Lerner Research Institute, Cleveland Clinic, Cleveland, OH 44196; [d]Department of Pharmacology, Case Western Reserve University, Cleveland, OH 44106; and [e]Department of Chemistry, University of Chicago, Chicago, IL 60637

Author contributions: Z.L., S.L., T.T.P., and T.S.X. designed research; Z.L., S.L., C.W., K.V., S.B., L.L., B.W., and T.S.X. performed research; T.L. and B.C.D. contributed new reagents/analytic tools; Z.L., S.L., C.W., K.V., M.M., A.O., T.T.P., and T.S.X. analyzed data; and Z.L., S.L., T.T.P., and T.S.X. wrote the paper.

1. K. Schroder, J. Tschopp, The inflammasomes. *Cell* **140**, 821–832 (2010).
2. E. Latz, T. S. Xiao, A. Stutz, Activation and regulation of the inflammasomes. *Nat. Rev. Immunol.* **13**, 397–411 (2013).
3. H. Guo, J. B. Callaway, J. P. Y. Ting, Inflammasomes: Mechanism of action, role in disease, and therapeutics. *Nat. Med.* **21**, 677–687 (2015).
4. J. Shi *et al.*, Cleavage of GSDMD by inflammatory caspases determines pyroptotic cell death. *Nature* **526**, 660–665 (2015).
5. N. Kayagaki, I. B. Stowe, B. L. Lee, K. O'Rourke, Caspase-11 cleaves gasdermin D for non-canonical inflammasome signalling. *Nature* **526**, 666–671 (2015).
6. W.-T. He *et al.*, Gasdermin D is an executor of pyroptosis and required for interleukin-1β secretion. *Cell Res.* **25**, 1285–1298 (2015).
7. N. Saeki, Y. Kuwahara, H. Sasaki, H. Satoh, T. Shiroishi, Gasdermin (Gsdm) localizing to mouse Chromosome 11 is predominantly expressed in upper gastrointestinal tract but significantly suppressed in human gastric cancer cells. *Mamm. Genome* **11**, 718–724 (2000).
8. P. Broz, P. Pelegrín, F. Shao, The gasdermins, a protein family executing cell death and inflammation. *Nat. Rev. Immunol.* **20**, 143–157 (2020).
9. J. Ding *et al.*, Pore-forming activity and structural autoinhibition of the gasdermin family. *Nature* **535**, 111–116 (2016).
10. X. Liu *et al.*, Inflammasome-activated gasdermin D causes pyroptosis by forming membrane pores. *Nature* **535**, 153–158 (2016).
11. R. A. Aglietti *et al.*, GsdmD p30 elicited by caspase-11 during pyroptosis forms pores in membranes. *Proc. Natl. Acad. Sci. U.S.A.* **113**, 7858–7863 (2016).
12. L. Sborgi *et al.*, GSDMD membrane pore formation constitutes the mechanism of pyroptotic cell death. *EMBO J.* **35**, 1766–1778 (2016).
13. X. Chen *et al.*, Pyroptosis is driven by non-selective gasdermin-D pore and its morphology is different from MLKL channel-mediated necroptosis. *Cell Res.* **26**, 1007–1020 (2016).
14. J. Shi, W. Gao, F. Shao, Pyroptosis: Gasdermin-mediated programmed necrotic cell death. *Trends Biochem. Sci.* **42**, 245–254 (2017).
15. S. Xia *et al.*, Gasdermin D pore structure reveals preferential release of mature interleukin-1. *Nature* **593**, 607–611 (2021).
16. P. Orning *et al.*, Pathogen blockade of TAK1 triggers caspase-8–dependent cleavage of gasdermin D and cell death. *Science* **362**, 1064–1069 (2018).
17. H. Kambara *et al.*, Gasdermin D exerts anti-inflammatory effects by promoting neutrophil death. *Cell Rep.* **22**, 2924–2936 (2018).
18. J. Sarhan *et al.*, Caspase-8 induces cleavage of gasdermin D to elicit pyroptosis during *Yersinia* infection. *Proc. Natl. Acad. Sci. U.S.A.* **115**, E10888–E10897 (2018).
19. S. S. Burgener *et al.*, Cathepsin G inhibition by Serpinb1 and Serpinb6 prevents programmed necrosis in neutrophils and monocytes and reduces GSDMD-driven inflammation. *Cell Rep.* **27**, 3646–3656.e5 (2019).
20. K. W. Chen *et al.*, Extrinsic and intrinsic apoptosis activate pannexin-1 to drive NLRP3 inflammasome assembly. *EMBO J.* **38**, e101638 (2019).
21. E. A. Miao *et al.*, Caspase-1–induced pyroptosis is an innate immune effector mechanism against intracellular bacteria. *Nat. Immunol.* **11**, 1136–1142 (2010).
22. Y. Aachoui, V. Sagulenko, E. A. Miao, K. J. Stacey, Inflammasome-mediated pyroptotic and apoptotic cell death, and defense against infection. *Curr. Opin. Microbiol.* **16**, 319–326 (2013).
23. I. Jorgensen, Y. Zhang, B. A. Krantz, E. A. Miao, Pyroptosis triggers pore-induced intracellular traps (PITs) that capture bacteria and lead to their clearance by efferocytosis. *J. Exp. Med.* **213**, 2113–2128 (2016).
24. J. Shi *et al.*, Inflammatory caspases are innate immune receptors for intracellular LPS. *Nature* **514**, 187–192 (2014).
25. N. Kayagaki *et al.*, Noncanonical inflammasome activation by intracellular LPS independent of TLR4. *Science* **341**, 1246–1249 (2013).
26. J. A. Hagar, D. A. Powell, Y. Aachoui, R. K. Ernst, E. A. Miao, Cytoplasmic LPS activates caspase-11: Implications in TLR4-independent endotoxic shock. *Science* **341**, 1250–1253 (2013).
27. V. A. K. Rathinam, Y. Zhao, F. Shao, Innate immunity to intracellular LPS. *Nat. Immunol.* **20**, 527–533 (2019).
28. X. Liu, J. Lieberman, A mechanistic understanding of pyroptosis: The fiery death triggered by invasive infection. *Adv. Immunol.* **135**, 81–117 (2017).
29. N. Van Opdenbosch, M. Lamkanfi, Caspases in cell death, inflammation, and disease. *Immunity* **50**, 1352–1364 (2019).
30. Y. Ma *et al.*, Research progress of the relationship between pyroptosis and disease. *Am. J. Transl. Res.* **10**, 2213–2219 (2018).
31. J. M. Hansen *et al.*, Pathogenic ubiquitination of GSDMB inhibits NK cell bactericidal functions. *Cell* **184**, 3178–3191.e18 (2021).
32. G. Luchetti *et al.*, Shigella ubiquitin ligase IpaH7.8 targets gasdermin D for degradation to prevent pyroptosis and enable infection. *Cell Host Microbe* **29**, 1521–1530.e10 (2021).
33. L. Hu *et al.*, Chemotherapy-induced pyroptosis is mediated by BAK/BAX-caspase-3-GSDME pathway and inhibited by 2-bromopalmitate. *Cell Death Dis.* **11**, 1–17 (2020).
34. A. G. Johnson *et al.*, Bacterial gasdermins reveal an ancient mechanism of cell death. *Science* **375**, 221–225 (2022).
35. J. K. Rathkey *et al.*, Chemical disruption of the pyroptotic pore-forming protein gasdermin D inhibits inflammatory cell death and sepsis. *Sci. Immunol.* **3**, eaat2738 (2018).
36. J. J. Hu *et al.*, FDA-approved disulfiram inhibits pyroptosis by blocking gasdermin D pore formation. *Nat. Immunol.* **21**, 736–745 (2020).
37. P. Devant *et al.*, Gasdermin D pore-forming activity is redox-sensitive. *Cell Rep.* **42**, 112008 (2023).
38. Z. Liu *et al.*, Crystal structures of the full-length murine and human gasdermin D reveal mechanisms of autoinhibition, lipid binding, and oligomerization. *Immunity* **51**, 43–49.e4 (2019).
39. J. Ruan, S. Xia, X. Liu, J. Lieberman, H. Wu, Cryo-EM structure of the gasdermin A3 membrane pore. *Nature* **557**, 62–67 (2018).
40. F. Humphries *et al.*, Succination inactivates gasdermin D and blocks pyroptosis. *Science* **369**, 1633–1637 (2020).
41. M. E. Linder, R. J. Deschenes, Palmitoylation: Policing protein stability and traffic. *Nat. Rev. Mol. Cell Biol.* **8**, 74–84 (2007).
42. Y. Fukata, M. Fukata, Protein palmitoylation in neuronal development and synaptic plasticity. *Nat. Rev. Neurosci.* **11**, 161–175 (2010).
43. C. Aicart-Ramos, R. A. Valero, I. Rodriguez-Crespo, Protein palmitoylation and subcellular trafficking. *Biochim. Biophys. Acta (BBA): Biomembr.* **1808**, 2981–2994 (2011).
44. T. Lanyon-Hogg, M. Faronato, R. A. Serwa, E. W. Tate, Dynamic protein acylation: New substrates, mechanisms, and drug targets. *Trends Biochem. Sci.* **42**, 566–581 (2017).
45. H. Jiang *et al.*, Protein lipidation: Occurrence, mechanisms, biological functions, and enabling technologies. *Chem. Rev.* **118**, 919–988 (2018).
46. M. S. Rana, C.-J. Lee, A. Banerjee, The molecular mechanism of DHHC protein acyltransferases. *Biochem. Soc. Trans.* **47**, 157–167 (2019).
47. M. Fukata, Y. Fukata, H. Adesnik, R. A. Nicoll, D. S. Bredt, Identification of PSD-95 palmitoylating enzymes. *Neuron* **44**, 987–996 (2004).
48. S.-A. Azizi *et al.*, Development of an acrylamide-based inhibitor of protein S-acylation. *ACS Chem. Biol.* **16**, 1546–1556 (2021).
49. Y. Webb, L. Hermida-Matsumoto, M. D. Resh, Inhibition of protein palmitoylation, raft localization, and T cell signaling by 2-bromopalmitate and polyunsaturated fatty acids. *J. Biol. Chem.* **275**, 261–270 (2000).
50. A. Daskalov, N. L. Glass, Gasdermin and Gasdermin-like pore-forming proteins in invertebrates, fungi and bacteria. *J. Mol. Biol.* **434**, 167273 (2022).
51. X. Wang *et al.*, Characterization of GSDME in amphioxus provides insights into the functional evolution of GSDM-mediated pyroptosis. *PLoS Biol.* **21**, e3002062 (2023).
52. A. G. Johnson *et al.*, Structure and assembly of a bacterial gasdermin pore. bioRxiv [Preprint] (2023). https://www.biorxiv.org/content/10.1101/2023.04.20.537723v1 (Accessed 13 May 2023).
53. J. Wan, A. F. Roth, A. O. Bailey, N. G. Davis, Palmitoylated proteins: Purification and identification. *Nat. Protoc.* **2**, 1573–1584 (2007).
54. R. Kang *et al.*, Neural palmitoyl-proteomics reveals dynamic synaptic palmitoylation. *Nature* **456**, 904–909 (2008).
55. Y. Liu, D. A. Fisher, D. R. Storm, Analysis of the palmitoylation and membrane targeting domain of neuromodulin (GAP-43) by site-specific mutagenesis. *Biochemistry* **32**, 10714–10719 (1993).
56. D. Popov-Čeleketić, F. Bianchi, S. J. Ruiz, F. Meutiawati, B. Poolman, A plasma membrane association module in yeast amino acid transporters. *J. Biol. Chem.* **291**, 16024–16037 (2016).
57. H. McClafferty, M. J. Shipston, "siRNA knockdown of mammalian zDHHCs and validation of mRNA expression by RT-qPCR" in *Protein Lipidation: Methods and Protocols. Methods in Molecular Biology*, M. E. Linder, Ed. (Springer, 2019), pp. 151–168.
58. A. Balasubramanian *et al.*, The palmitoylation of gasdermin D directs its membrane translocation and pore formation during pyroptosis. *Sci. Immunol.* **9**, eadn1452 (2024).
59. A. G. Johnson *et al.*, Structure and assembly of a bacterial gasdermin pore. *Nature* **628**, 657–663 (2024).
60. S. Rühl *et al.*, ESCRT-dependent membrane repair negatively regulates pyroptosis downstream of GSDMD activation. *Science* **362**, 956–960 (2018).
61. K. Nozaki *et al.*, Caspase-7 activates ASM to repair gasdermin and perforin pores. *Nature* **606**, 960–967 (2022).
62. M. F. Schmidt, M. Bracha, M. J. Schlesinger, Evidence for covalent attachment of fatty acids to Sindbis virus glycoproteins. *Proc. Natl. Acad. Sci. U.S.A.* **76**, 1687–1691 (1979).
63. O. Rocks *et al.*, An acylation cycle regulates localization and activity of palmitoylated Ras isoforms. *Science* **307**, 1746–1752 (2005).
64. L. Wang *et al.*, Palmitoylation prevents sustained inflammation by limiting NLRP3 inflammasome activation through chaperone-mediated autophagy. *Mol. Cell* **83**, 281–297.e10 (2023).
65. Y. Lu *et al.*, Palmitoylation of NOD1 and NOD2 is required for bacterial sensing. *Science* **366**, 460–467 (2019).
66. K. Mukai *et al.*, Activation of STING requires palmitoylation at the Golgi. *Nat. Commun.* **7**, 11932 (2016).
67. H. T. Nguyen *et al.*, Spike glycoprotein and host cell determinants of SARS-CoV-2 entry and cytopathic effects. *J. Virol.* **95**, e02304-20 (2021), 10.1128/jvi.02304-20.
68. F. S. Mesquita *et al.*, S-acylation controls SARS-CoV-2 membrane lipid organization and enhances infectivity. *Dev. Cell* **56**, 2790–2807.e8 (2021).
69. R. Puthenveetil *et al.*, S-acylation of SARS-CoV-2 spike protein: Mechanistic dissection, in vitro reconstitution and role in viral infectivity. *J. Biol. Chem.* **297**, 101112 (2021).
70. G. Du *et al.*, ROS-dependent S-palmitoylation activates cleaved and intact gasdermin D. *Nature* **630**, 437–446 (2024), 10.1038/s41586-024-07373-5.
71. N. Zhang *et al.*, A palmitoylation–depalmitoylation relay spatiotemporally controls GSDMD activation in pyroptosis. *Nat. Cell Biol.* **26**, 757–769 (2024), 10.1038/s41556-024-01397-9.
72. M. I. P. Malgapo, M. E. Linder, Substrate recruitment by zDHHC protein acyltransferases. *Open Biol.* **11**, 210026 (2021).
73. C. A. Ocasio *et al.*, A palmitoyl transferase chemical–genetic system to map ZDHHC-specific S-acylation. *Nat. Biotechnol.*, 10.1038/s41587-023-02030-0 (2024).
74. K. Wang *et al.*, Structural mechanism for GSDMD targeting by autoprocessed caspases in pyroptosis. *Cell* **180**, 941–955.e20 (2020).
75. Z. Liu *et al.*, Caspase-1 engages full-length Gasdermin D through two distinct interfaces that mediate caspase recruitment and substrate cleavage. *Immunity* **53**, 106–114 (2020).
76. H. Yin *et al.*, Insights into the GSDMB-mediated cellular lysis and its targeting by IpaH7.8. *Nat. Commun.* **14**, 61 (2023).
77. C. Wang *et al.*, Structural basis for GSDMB pore formation and its targeting by IpaH7.8. *Nature* **616**, 590–597 (2023).
78. X. Zhong *et al.*, Structural mechanisms for regulation of GSDMB pore-forming activity. *Nature* **616**, 598–605 (2023).
79. C. G. Weindel *et al.*, Mitochondrial ROS promotes susceptibility to infection via gasdermin D-mediated necroptosis. *Cell* **185**, 3214–3231.e23 (2022).
80. J. Guo *et al.*, Resin-assisted enrichment of thiols as a general strategy for proteomic profiling of cysteine-based reversible modifications. *Nat. Protoc.* **9**, 64–75 (2014).
81. D. De Nardo, D. V. Kalvakolanu, E. Latz, "Immortalization of murine bone marrow-derived macrophages" in *Macrophages: Methods and Protocols. Methods in Molecular Biology*, G. Rousselet, Ed. (Springer, 2018), pp. 35–49.